Draft version July 27, 2019
Typeset using LaTeX **twocolumn** style in AASTeX62

The Role of X-ray Luminous AGN in Quenching the Main Sequence

Christopher E. Bain[1] and David Sanders[2]

[1] *University of Maryland Baltimore County, 1000 Hilltop Circle, Baltimore, MD 21250, USA*
[2] *Institute of Astronomy, 2680 Woodlawn Dr, Honolulu, HI 96822, USA*

ABSTRACT

We investigated a sample of 3259 luminous X-ray sources from the COSMOS survey with redshift ($z < 4$) to determine if AGN activity quenches star-formation in galaxies. We produced new model-free estimates of star-formation rate (SFR) and stellar mass ($M_\star$) to which we then compared the position of the X-ray sources in the $SFR - M_\star$ diagram with measurements of the galaxy "Main Sequence" (MS) from the literature. We found that star-formation rates derived from Ultraviolet (UV) to Near-infrared (NIR) SED-fitting tend to dramatically overestimate star-formation in X-ray sources. All X-ray sources, independent of spectral type, lie below the MS with SFR increasing as a function of $M_\star$. In addition, we found no correlation between offset in SFR from the MS (ΔSFR_{MS}) and X-ray luminosity, but found that the median ΔSFR_{MS} decreases as a function of $M_\star$. We conclude that accurate measurements of SFR for luminous X-ray AGN are essential for determining the role of AGN activity in quenching star-formation.

Keywords: main sequence — galaxies: active — galaxies: nuclei — galaxies: evoltuion

1. INTRODUCTION

Over the past decade, it has become clear that the star formation rate (SFR) and stellar mass ($M_\star$) of "star-forming galaxies" are highly correlated. Early studies revealed the existence of a roughly linear $SFR - M_\star$ relation, which was termed the star-forming galaxy "Main Sequence (MS)" (Noeske et al. 2007; Daddi et al. 2007; Elbaz et al. 2007). The salient features of the MS from these early studies are that normalization of the MS increases with redshift, while the intrinsic scatter in the relation is small ($0.2 - 0.3$ dex) at all redshifts studied (Speagle et al. 2014). It was argued that the existence of the MS implied that star-formation was regulated by a limited set of internal processes, (e.g. gas supply). Exhaustion of a galaxy's gas supply would then lead to "quenching", transforming the galaxy in color from blue to red.

With the availability of data from the *Spitzer* and *Herschel* space telescopes, studies using large samples of robust mid- and far-IR based measurements uncovered a flattening, or "turnover", in the slope of the MS above $M_\star \sim 3 \times 10^{10}\ M_\odot$ in local galaxies (Salim et al. 2007) as well as at higher redshifts (Whitaker et al. 2014; Lee et al. 2015; Tomczak et al. 2016).

The existence of a turnover in the MS implies that massive galaxies have lower average SFRs than would be expected if there were a linear MS. Leslie et al. (2016) have analyzed the SFR data for Sloan Digital Sky Survey (SDSS) galaxies as a function of spectral type, and have shown that Composite (a combination of star-forming and low-energy galaxies), Seyfert 2 (galaxies with quasar-like nuclei), and LINER (low-ionization galaxy with weakly-ionized or neutral atoms) galaxies form a "quenching pathway" for massive galaxies, which is nearly perpendicular to the star-forming MS, suggesting that active galactic nuclei (AGN) may play a key role in quenching star formation and removing massive galaxies from the MS.

Interactions of galaxies are essential in driving galaxy growth and transforming galaxy morphology. During violent encounters and mergers of galaxies, gas in the galaxy disks can lose angular momentum and sink to the center of the individual galaxies as well as the merger remnant (Hung et al. 2013). As a first step in determining the relative importance of galaxy interactions vs. secular processes, we need to quantify the morphological properties of individual sources. This is being done initially for the sample of ~ 4000 luminous X-ray AGN using high-resolution HST images, along with the visual morphological classification scheme that has been previously vetted on the much larger sample of Cosmic Evolution Survey (COSMOS) galaxies (Hung et al. 2013).

2. METHODOLOGY

By combining data from the Accretion History of AGN (AHA: http://project.ifa.hawaii.edu/aha/) Survey and the Cosmic Evolution Survey (COSMOS: http://cosmos.astro.caltech.edu/) we are able to extract accurate source positions, multi-wavelength photometry and optical images for all $\sim$ 4000 X-ray sources in the COSMOS/AHA catalogs. COSMOS is a deep, wide area (2-deg^2), multi-wavelength survey aimed at measuring the evolution of galaxies over cosmic time. The COSMOS survey is centered at (J2000): RA +150.119, DEC +2.2058. The field has been observed at all accessible wavelengths from the X-ray to the radio with most of the major space-based (*e.g. Hubble, Spitzer, GALEX, XMM, Chandra, Herschel, NuStar*) and ground based telescopes (e.g. Keck, Subaru, CFHT, ESO-VLT, UKIRT, NOAO-Badde+Blanco, VLA). More detailed information on the X-ray sources in the COSMOS catalog can also be found on the AHA website and in the original COSMOS-Chandra/XMM survey papers (Civano et al. 2016; Marchesi et al. 2016).

2.1. *Constructing the Galaxy Main Sequence*

Data from the COSMOS catalog will be used to construct the galaxy star-formation MS in six redshift bins: $(0.5 < z < 1)$, $(1 < z < 1.5)$, $(1.5 < z < 2)$, $(2 < z < 2.5)$, $(2.5 < z < 3)$. An example of what these plots will look like is shown in Figure 1, which was produced using galaxies in the SDSS at $z < 0.5$. Figure 1 illustrates the increasing "turnover" observed in SFR at high stellar mass as different spectral classes of narrow-line AGN are included in the total sample of "star-forming galaxies". These MS plots will **not include** any of our luminous X-ray AGN sources since sources with dominant AGN have, by definition, been excluded from the lists of "star-forming galaxies" in the COSMOS catalog.

2.2. *New Estimates $M_\star$ and SFR for Luminous AGN*

Robust SFR and $M_\star$ estimates are essential to analyze the position of galaxies in relation the MS. Standard SED fitting techniques that do no account for emission from the AGN accretion disk in the UV, known as the big-blue-bump (BBB) (Sanders et al. 1989; Elvis et al. 1994) tend to overestimate SFR and provide unpredictable estimates of $M_\star$. To provide better model-free estimates of SFR and $M_\star$, the well-studied galaxy Arp-200 was used to develop simple-scaling relations between 1 micron luminosity and $M_\star$ as well as 250 micron emission and SFR which are explained in detail below. $M_\star$ values were calculated by first constructing the spectral energy distribution (SED) for each source using the more recent (and more accurate) photometry that is being compiled for the next version of the COSMOS catalog (COSMOS2020, in preparation). Estimates for $M_\star$ were determined from the observed rest-frame 1 micron luminosity, while SFR were computed from the observed rest-frame far-infrared (FIR) luminosity. SFR values were calculated using SPIRE 250 micron data. Only $\sim$ 900 sources out of the 3600 sources had any detection in the 250 micron band. To calculate the new mass values we took the rest-frame νL_ν values at 1 micron and divided by 2.5. For the new SFR we took the observed 250 micron data, found the rest-frame νL_ν value for this observation, divided by 4 x 10^{12}, and then multiplied by 100. By using the 8 and 24 micron data, we extrapolated SFRs that did not previously have an SFR value. SFRs that are upper limits did not have 24 micron or 250 micron detections ($\sim$ 1100 sources).

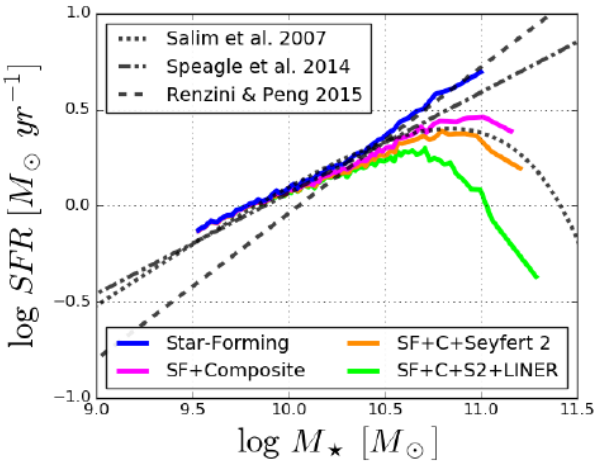

Figure 1. The median SFR as a function of $M_\star$ for galaxies in four subsets of spectral classes (coloured lines). The dashed and dotted lines show measurements from the studies indicated at the top left. (McPartland et al. 2019; Renzini & Peng 2015)

3. RESULTS

The MS for each of our six redshift bins, (see Figures 2, 3, and 4) was determined using the "All Galaxies" (Equation 3) in Tomczak et al. (Tomczak et al. 2016). The median SFR and 25% and 75% range of values were determined for five stellar mass bins, $M_\star$ = 9.5-10, 10-10.5, 10.5-11, 11-11.5, and 11.5-12.

Figure 5 shows the comparison of the original data in the Marchesi catalog (Marchesi et al. 2016) to the recalculated values we accomplished. The $(0.5 < z < 1)$ redshift bin contained the most amount of X-ray sources for each data group and was the most valid comparison between both. The Marchesi data contained 694 sources whereas the recalculated graph contained 684 sources.

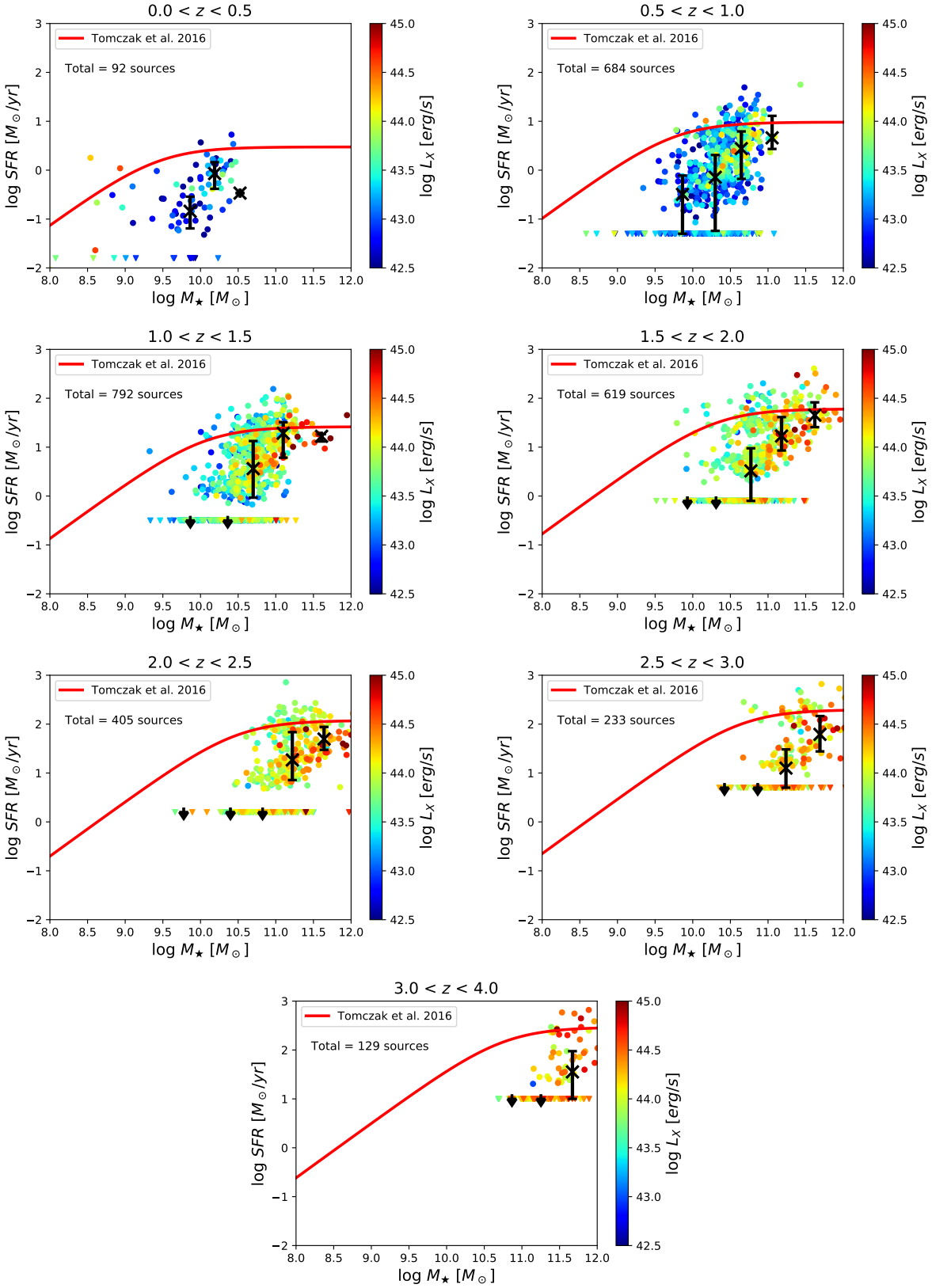

Figure 2. SFR versus $M_\star$ for all 3259 luminous X-ray sources. Sources have been binned in redshift as indicated on each of the 7 panels. The solid red line represents the galaxy "Main Sequence" as determined by Tomczak et al. (Tomczak et al. 2016) for each redshift bin. "X" symbols and vertical bars represent the median and 25% − 75% range of SFR in 5 stellar mass bins, 9.5-10, 10-10.5, 10.5-11, 11-11.5, 11.5-12. Upper limits are designated as downward triangles; these are SFRs that had no detection in 24 or 250 micron flux bands.

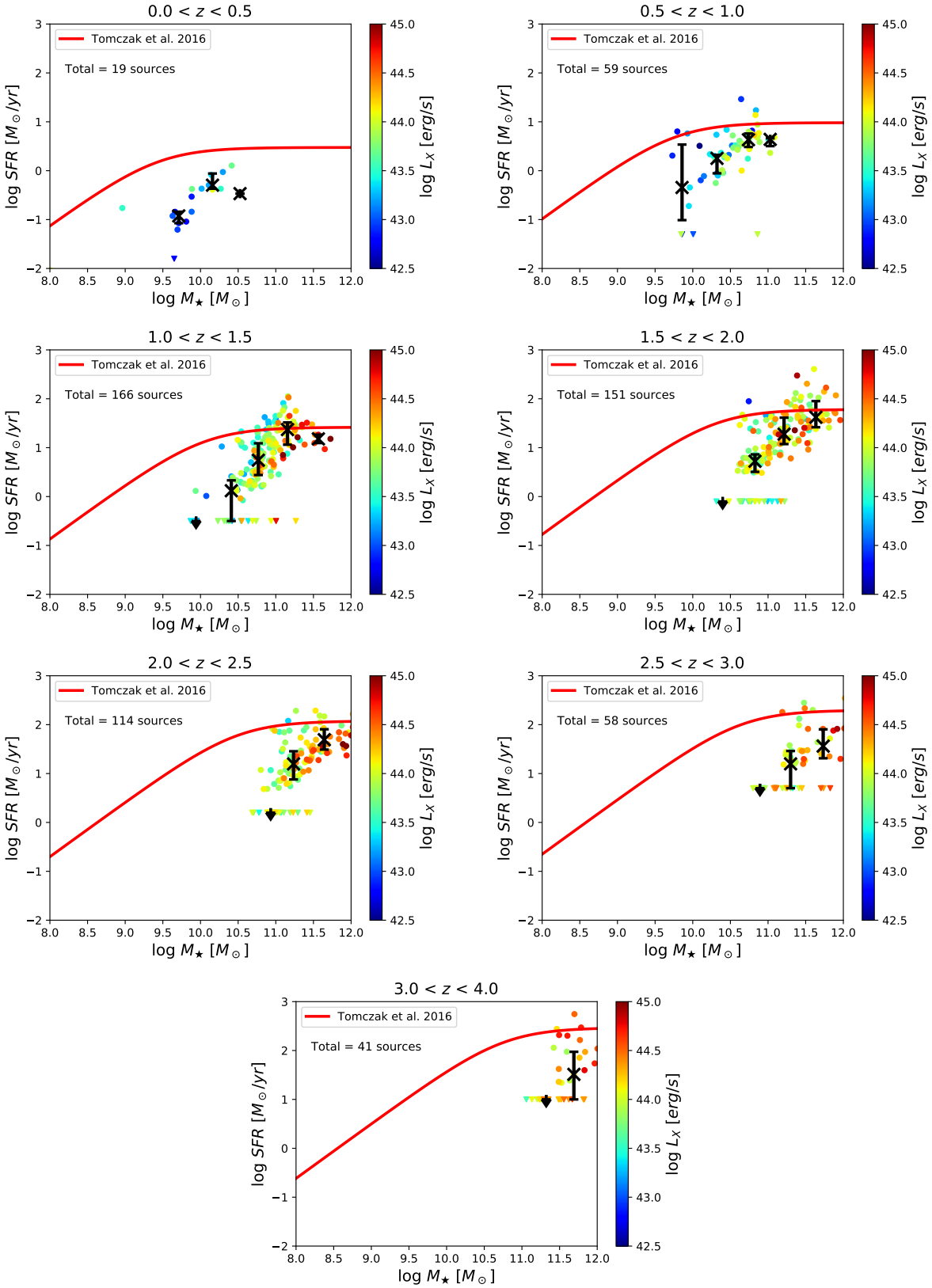

Figure 3. Same as Figure [2] except for Type 1 sources only.

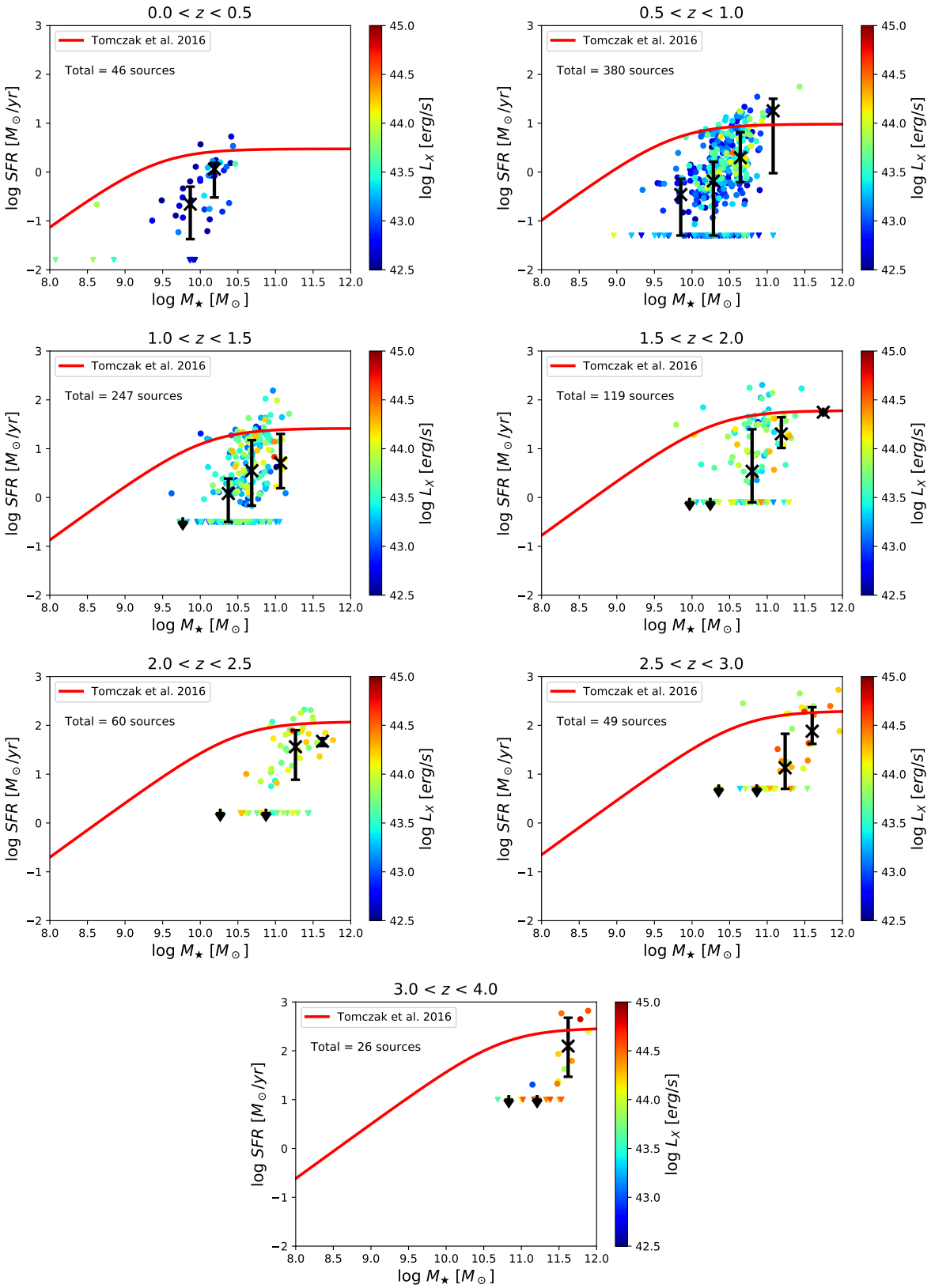

Figure 4. Same as Figure [2] except for Type 2 sources only.

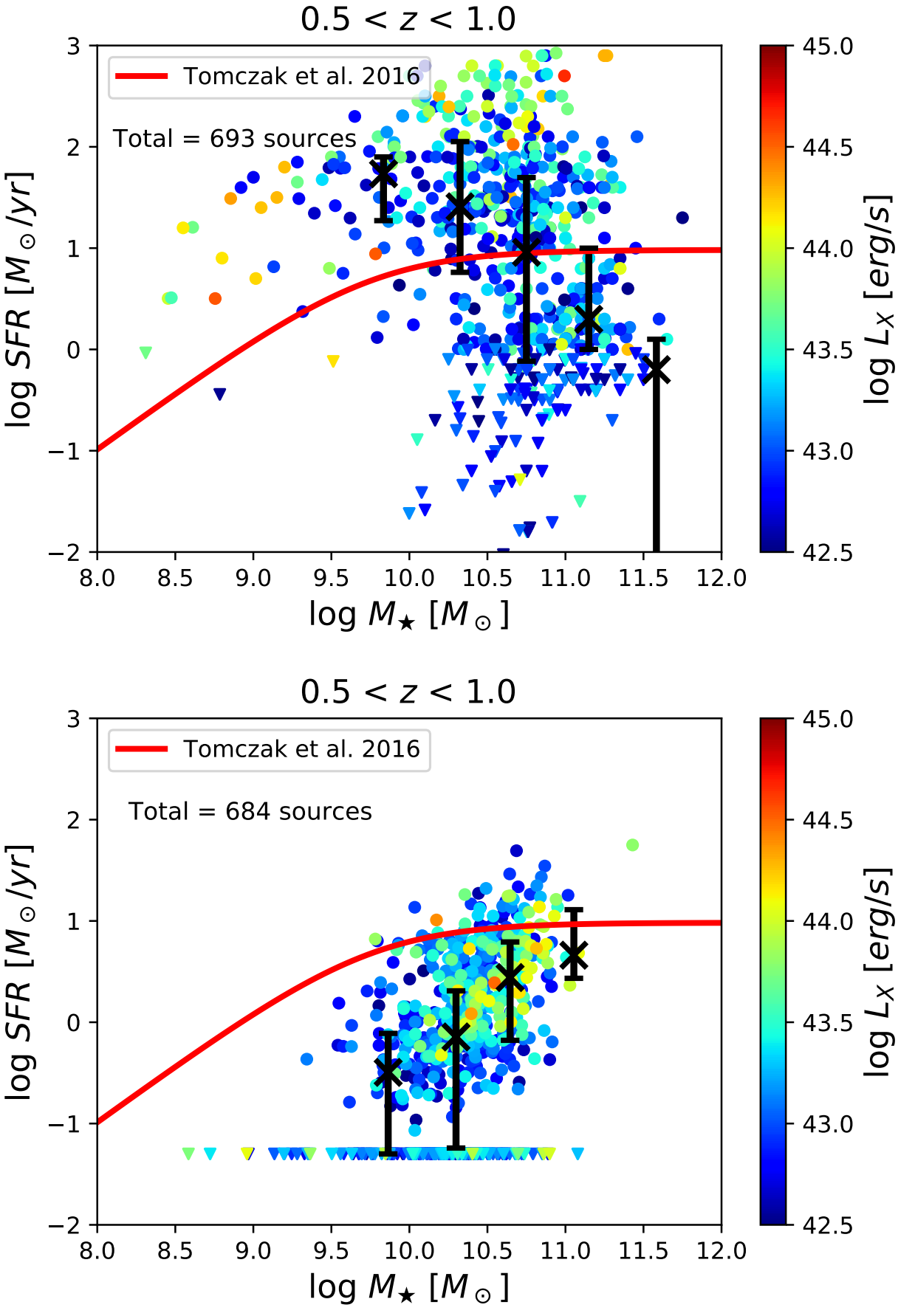

Figure 5. Distribution source comparison between COSMOS2015 catalog and recomputed sources.

After recalculation of $M_\star$ and SFR for each Marchesi source using their 24 and 250 micron flux detections, we used the same process to bin the sources by their redshifts. Figures 2, 3, and 4 show the results for 3259 sources that had both detections in 24 and 250 micron flux bands. The number of sources in each redshift bin was 92 ($0 < z < 0.5$), 684 ($0.5 < z < 1$), 792 ($1 < z < 1.5$), 619 ($1.5 < z < 2$), 405 ($2 < z < 2.5$), 233 ($2.5 < z < 3$), and 129 ($3 < z < 3.5$). About $\sim 47\%$ (1535) of the sources were able to be classified as Type 1 (608) or Type 2 (927). For Type 1 sources, the number of sources in each redshift bin was 19 ($0 < z < 0.5$), 59 ($0.5 < z < 1$), 166 ($1 < z < 1.5$), 151 ($1.5 < z < 2$), 114 ($2 < z < 2.5$), 58 ($2.5 < z < 3$), and 41 ($3 < z < 3.5$). For Type 2 sources, the number of sources in each redshift bin was 48 ($0 < z < 0.5$), 380 ($0.5 < z < 1$), 247 ($1 < z < 1.5$), 119 ($1.5 < z < 2$), 60 ($2 < z < 2.5$), 49 ($2.5 < z < 3$), and 26 ($3 < z < 3.5$).

4. DISCUSSION

4.1. *SFR and $M_\star$ Estimates in the COSMOS2015 Catalog*

After quick inspection of the data of the COSMOS2015 catalog, it was observed that there were a large number of sources that were missing SFRs. In addition to this, all sources that did not contain SFRs also did not contain $M_\star$ values and could not be displayed.

Figure 5 shows that the median SFR within each mass bin, in general, follows the shape of the MS; suggesting that the luminous X-ray AGN exhibit similar SFR as the population of non-AGN (i.e. the "star-forming" galaxy population). However, there are clearly exceptions as illustrated by the negative slope of SFR vs. $M_\star$ for all galaxies in the ($0.5 < z < 1$) redshift bin (see upper left panel in Figure 5).

After further inspection of Figure 5, we noticed, in several redshift bins, two common disagreements with the data: (1) the distribution of sources in all redshift bins showed a negative slope which did not follow the MS, (2) several low-mass ($M_\star = 8 - 10$) sources displayed abnormally high SFR values ($1.1 - 2\ M_\odot \cdot yr^{-1}$), which were significantly higher than the MS. After looking into the methodology of calculations behind the COSMOS2015 catalog, we found that their method of using multi-component SED templates in both NIR and FIR to UV to fit the overall observed SEDs produced a relatively large number of abnormal values for SFR. Most notably by assuming that any observed UV radiation was from star formation, rather than the emergence of the BBB. We then decided that recalculation was needed for both $M_\star$ and SFR. Furthermore, more robust IR from the *Herschel* telescope could have been used in the COSMOS2015 catalog to produce more accurate SFR values, however, was not used. Suh et al. (2019) used the *Herschel* -detected sources to create similar $SFR - M_\star$ plots, however since we were not using *Herschel* data, we wanted to display data that not not only contained proper SFR and $M_\star$ estimates, but also created a simple and independent way of checking the results of Suh et al. (2019).

4.2. *COSMOS2015 Catalog Versus Computed Values for SFR and $M_\star$*

After recalculation of SFR and $M_\star$ we compared our revised source graph to original COSMOS2015 catalog distribution where we observed dramatic changes between each. The negative slope in the distribution of points adjusted to positive, displayed by the median values in the plots. In addition to this, low-mass sources ($M_\star = 8 - 10$) no longer displayed abnormally high SFR values and lied below the MS. Furthermore, our revised graph no longer displayed significant outliers to the MS; in that most sources now lay on average of 0.1 dex below the MS. Finally, proper upper limits were displayed for the recalculated sources making correct median lines for the plot in comparison to the COSMOS2015 distribution whereas median lines were skewed.

4.3. *Investigating Correlations between Main Sequence Offset as a function of L_X and $M_\star$*

The Main Sequence offset (ΔSFR_{MS}) is defined as the distance an X-ray source deviates from the expected displayed MS line (Tomczak et al. 2016; Suh et al. 2019). Using ΔSFR_{MS} gives a proper estimate for what we would believe to see for galaxies that do not lie along the MS. Therefore, we use ΔSFR_{MS} as a function of its star-formation history to investigate potential correlations.

We show in Figure 6 ΔSFR_{MS} as a function of X-ray Luminosity (L_X). We discovered no clear correlation between ΔSFR_{MS} and L_X for all X-ray sources as well as when divided into spectral type.

In Figure 7, we displayed ΔSFR_{MS} as a function of stellar mass ($M_\star$) and observed a distinct correlation. The median ΔSFR_{MS} value decreased towards the $\Delta SFR_{MS} = 0$ line. Additionally, when separated into spectral type, the correlation is upheld.

5. CONCLUSIONS

We used a sample of luminous X-ray AGN from the COSMOS survey to determine if AGN activity quenches star-formation in galaxies. To accomplish this, we produced new robust model-free estimates of star-formation

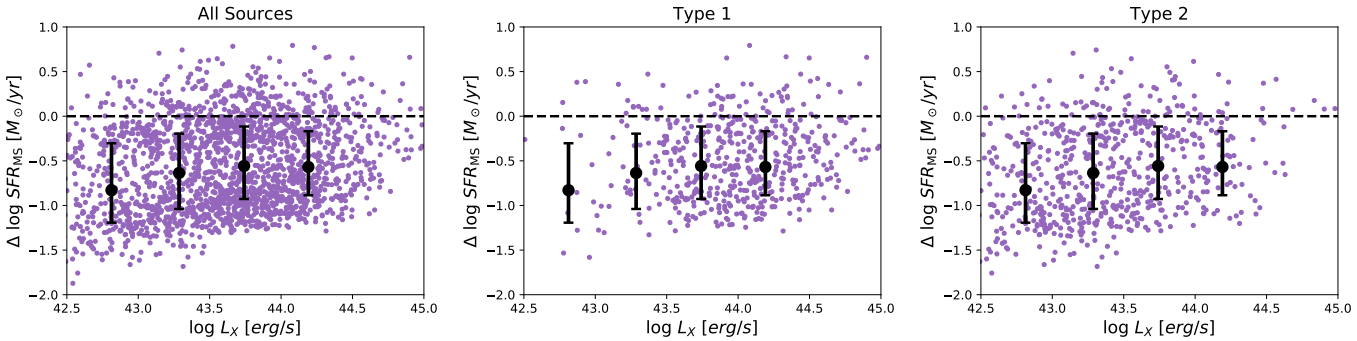

Figure 6. Offset in SFR from the MS (ΔSFR_{MS}) as a function of X-ray Luminosity. Black dots and vertical bars represent the median and 25% − 75% range of ΔSFR_{MS}. Dashed black line represents $\Delta SFR_{MS} = 0$.

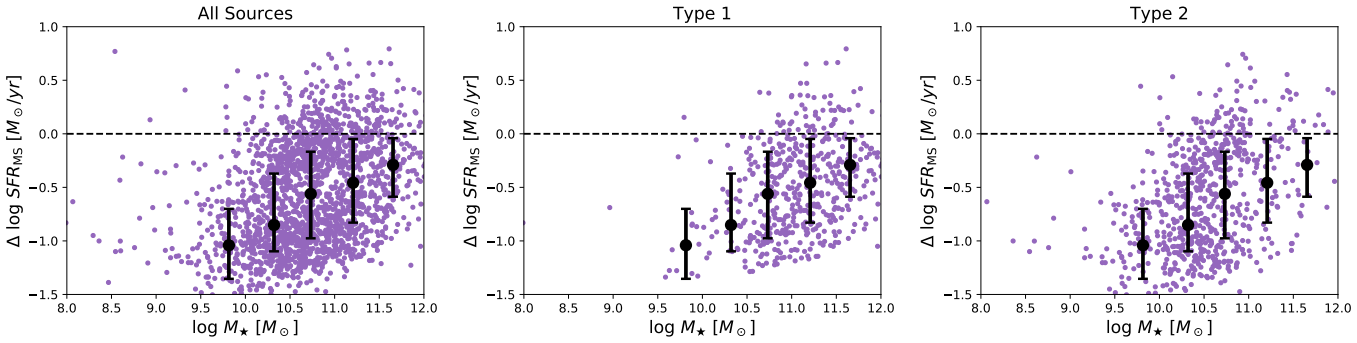

Figure 7. Same as Figure 6 except for ΔSFR_{MS} as a function of $M_\star$.

rate and stellar mass for our sample of X-ray detected galaxies. We then compared the position of the X-ray sources in the $SFR - M_\star$ diagram with measurements of the galaxy Main Sequence from the literature. To further investigate if AGN activity quenches star-formation, we analyzed the offsets from the Main Sequence in SFR as a function of X-ray Luminosity and stellar mass. Our main results are summarized below:

- Star-formation rates derived from UV to NIR SED fitting tend to drastically overestimate the amount of star-formation in luminous X-ray sources. However, simple estimates based on the observed 250 micron luminosities provide more robust estimates.
- Sources in all redshift bins lie below the Main Sequence with SFR increasing as a function of stellar mass.
- Splitting sources by spectral classification into Type 1 and Type 2 AGN show no significant difference in position in relation to the Main Sequence.
- We find little to no correlation between X-ray Luminosity and offset in SFR from the Main Sequence for all X-ray sources as well as when divided by spectral type.
- The median offset in SFR from the Main Sequence decreases as a function of stellar mass for all X-ray sources as well as when divided by spectral type.

It is clear from this analysis that accurate measurements of star-formation rates for luminous X-ray AGN are essential for determining the role of AGN activity in quenching star-formation. Additional deeper FIR data would help to address this issue, but will have to wait for the next generation of FIR space telescopes. In the mean time, a more in-depth treatment of upper limits on star-formation rate derived from FIR fluxes is needed to progress our understanding of the relationship between AGN activity and quenching.

6. ACKNOWLEDGEMENTS

Christopher Bain (CB) and David Sanders (DS) acknowledge support from Research Experience for Undergraduate program at the Institute for Astronomy, University of Hawaii-Manoa funded through NSF grant 6104374. CB and DS would also like to thank the Institute for Astronomy for their kind hospitality during the course of this project and NSF award number 1716994 for financial support.

REFERENCES

Civano, F., Marchesi, S., Comastri, A., et al. 2016, ApJ, 819, 62

Daddi, E., Dickinson, M., Morrison, G., et al. 2007, ApJ, 670, 156

Elbaz, D., Daddi, E., Le Borgne, D., et al. 2007, A&A, 468, 33

Elvis, M., Wilkes, B. J., McDowell, J. C., et al. 1994, ApJS, 95, 1

Hung, C.-L., Sanders, D. B., Casey, C. M., et al. 2013, ApJ, 778, 129

Lee, N., Sanders, D. B., Casey, C. M., et al. 2015, ApJ, 801, 80

Leslie, S. K., Kewley, L. J., Sanders, D. B., & Lee, N. 2016, MNRAS, 455, L82

Marchesi, S., Civano, F., Elvis, M., et al. 2016, ApJ, 817, 34

McPartland, C., Sanders, D. B., Kewley, L. J., & Leslie, S. K. 2019, MNRAS, 482, L129

Noeske, K. G., Faber, S. M., Weiner, B. J., et al. 2007, ApJL, 660, L47

Renzini, A., & Peng, Y.-j. 2015, ApJ, 801, L29

Salim, S., Rich, R. M., Charlot, S., et al. 2007, ApJS, 173, 267

Sanders, D. B., Phinney, E. S., Neugebauer, G., Soifer, B. T., & Matthews, K. 1989, ApJ, 347, 29

Speagle, J. S., Steinhardt, C. L., Capak, P. L., & Silverman, J. D. 2014, ApJS, 214, 15

Suh, H., Civano, F., Hasinger, G., et al. 2019, ApJ, 872, 168

Tomczak, A. R., Quadri, R. F., Tran, K.-V. H., et al. 2016, ApJ, 817, 118

Whitaker, K. E., Franx, M., Leja, J., et al. 2014, ApJ, 795, 104